Laser remote sensing of species concentrations and dynamical processes

C. Russell Philbrick[*a.b] and Hans D. Hallen[a]
[a]Physics Department and [b]MEAS Department, N.C. State University, Raleigh NC 27695

ABSTRACT

A review of current lidar techniques summarizes present capabilities to: (1) measure atmospheric concentrations of most major and several minor molecular species using Raman scattering and DIAL techniques, (2) detect and measure concentrations of certain trace level species, (3) characterize active dynamical processes in the troposphere based upon using water vapor as a tracer, and (4) describe interesting thermodynamic properties based upon rotational Raman temperature profiles, multi-wavelength aerosol distributions, and changes in the phase states of water. Advances in lasers and detectors have extended the range of wavelengths available through the ultraviolet, visible, and infrared spectrum by using tunable laser techniques and supercontinuum broad spectrum lasers. Prior studies are reviewed, several applications for the technology are suggested which extend the techniques proposed to future investigations. In particular, the extension of tunable laser sources into the ultraviolet region has opened opportunities to use resonance Raman techniques, which provide greatly increased sensitivity for certain molecular species, such as hydrocarbons. The developments of supercontinuum lasers and tunable OPO lasers has enabled long-path trace concentration measurements of molecular spectra lines to detect and measure the concentrations of many species, as well as to distinguish any interfering species.

Keywords: Raman Lidar, DIAL, Supercontinuum Absorption Lidar, Resonance Raman, Atmospheric Chemistry, Atmospheric Dynamics, Optical Extinction

1. INTRODUCTION

An overview of several earlier measurements using laser remote sensing techniques provides a description of our current ability to measure atmospheric properties. Several of these example measurements are selected to show a few selected scientifically interesting results, and to demonstrate the capabilities that presently exist. Advancements in lasers and detectors during the last few years open new opportunities to measure the properties of the lower atmosphere, such as profiling the chemical species and aerosol concentrations, following the dynamical processes of convective mixing and turbulence, examining the microphysical thermal processes that govern cloud formation and phase state changes, and detecting trace concentrations of chemical species resulting from industrial air pollution and biogenic processes. Wavelength tunable lasers and broad band supercontinuum lasers open opportunities to measure resonance Raman processes in the UV region and molecular absorption techniques at infrared wavelengths, these techniques now allow measurements of trace levels of chemical species using the unique spectral signatures resulting from optical scattering and absorption of molecules. Dynamical processes in the lower atmosphere are studied by using water vapor as a tracer of dynamics; examples of daytime convection, weather front motion, Boer waves, and cloud convection are examined. The microphysical thermodynamic processes that result in cloud formation can be studied using Raman lidar measurements of temperature and water vapor distribution surrounding cloud formations, the particle size changes observed using multi-wavelength measurements of optical extinction, and detecting phase changes of water. The relative variations between the vapor, liquid and solid phases of water can be observed in the Raman spectra; these exhibit wavelength shifts of the Raman scatter signature caused by changes in bond strengths. The measurements of the evolving physical properties of clouds and studies of processes in the growth and dissipation of clouds should help in better understanding the radiative forcing that is still of much concern in climate change studies. The many different properties that can be simultaneously measured using a Raman lidar make it a valuable tool for these investigations.

*philbrick**@ncsu.edu;** phone 1 919 513-7174

Laser Radar Technology and Applications XIX; and Atmospheric Propagation XI, edited by Monte D. Turner, Gary W. Kamerman, Linda M. Wasiczko Thomas, Earl J. Spillar, Proc. of SPIE Vol. 9080, 90800Z
 · doi: 10.1117/12.2050696

The first Raman measurements of atmospheric properties with lidar were carried out in the late 1960's by Leonard [1] and Cooney [2]. Two years later, Melfi et al. [3] and Cooney [4,5] showed that it was possible to measure water vapor profiles using the Raman lidar technique. A significant contribution made by Inaba and Kobayasi [6] who suggested in 1972 that many different molecular species could be measured using vibrational Raman scattering. While early tests [3-5,7] showed that it was possible to measure the water vapor with limited range and accuracy, later investigations showed significant improvements. Many groups began making use of the capabilities of Raman lidar for measurements of the atmosphere during the 1980's; a useful summary of activities for water vapor measurements by DIAL and Raman lidar was given by Grant [8]. Also, this period included development of the rotational Raman lidar to profile temperature, beginning with an early measurement by Arshinov et al. [9]. Summaries with examples of some of these developments in the 1980's and 90's have been prepared [13-15]. Lidar investigations during this period also focused on measuring the middle atmosphere density variations due to gravity and planetary waves, aerosols introduced into the stratosphere by volcanic activity, and temperature profiles through the mesosphere and stratosphere [16-22]. During the 1990's, several research groups demonstrated convincingly that the Raman techniques provide accurate remote sensing measurements of water vapor and temperature profiles, with high temporal and spatial resolution [23-34].

Laser remote sensing techniques give the ability to investigate atmospheric processes, provide meteorological data, measure air quality, and monitor industrial and commercial chemicals in real time for extended periods of time. Examples of optical scattering measurements are presented here from our research using Rayleigh, Raman, and DIAL lidar instruments to show a portion of the wide range of atmospheric properties and applications. This paper also includes a brief look at several topics of more recent interest: air pollution events [36-40], aerosol profiling, bi-static aerosol characterization [15,44-49], resonance Raman for high sensitivity measurements [50], MWIR lidar for measurements of trace species [51], and long-path supercontinuum lasers [52-54]. The later two techniques advance the use of DIAL lidar techniques by taking advantage of new technologies. We conclude by showing a few examples of striking atmospheric features that deserve further investigation. This range of examples is intended to show the value of long time sequences of lidar measurements to study processes that cannot be observed using the snapshots from point sensors on balloons, met-rockets, and aircraft.

2. MEASUREMENT CAPABILITIES

Many simple Rayleigh lidar instruments, referred to as micro-pulse lidar, are deployed around the world today by meteorologists, as well as atmospheric researchers, who are interested in the information that can be gleaned from the backscatter profiles. A time sequence of the backscatter profiles provides a useful picture to describe the temporal changes in the aerosol scattering. Changes in the boundary layer are easily observed and even sub-visual clouds can be detected in the troposphere. A Rayleigh lidar is relatively inexpensive and is generally easy to operate. The results provide mostly a qualitative view of the atmosphere, although quantitative measurements of cloud height, boundary layer thickness, and relative changes in the aerosol backscatter intensity can be acquired. Figure 1 shows the measurements from an eye-safe micro-pulse lidar during a six-hour period between 8 AM and 2 PM local time (LT). The normal daytime growth of the boundary layer is observed as the convection cells generated by surface heating carry moisture aloft and generate aerosols in the cooler atmosphere above. These instruments provide an interesting picture of the time sequence of events as weather fronts approach, and indicate improving or worsening weather conditions. The Rayleigh lidar technique can also be used to study middle atmosphere properties, where the aerosol scattering component is very small. If one uses a larger laser transmitter and telescope receiver, the signal returns from the stratosphere and mesosphere can be used to study the wave variations in the density and measure atmospheric temperature profiles [16-22]. The temperature profile is calculated from the molecular profile gradient by integrating downward from the top of the backscatter profile using the hydrostatic equation in the aerosol-free regions of the stratosphere and mesosphere.

The Differential Absorption Lidar (DIAL) and Raman lidar techniques have been used for measuring gas concentrations in the lower atmosphere. DIAL uses two laser wavelengths to ratio signals of a molecular absorption line (on-line) with a nearby wavelength in a region of no absorption (off-line) in the backscatter profiles. An early comparison of the DIAL and Raman lidar techniques discussed the capabilities and limitations of each [8]. The DIAL technique had only limited application before the recent availability of tunable lasers, but the advent of optical parametric oscillators (OPO) and diode lasers made it easier to match a laser output with useful molecular absorption features. The advantage of DIAL over Raman lidar techniques is that the cross-sections for absorption are larger (1000X) compared to Raman scattering; however, output power typical of OPO lasers and diode lasers is relatively lower, and DIAL techniques rely on the presence of aerosol scattering. Also, Raman lidar can simultaneously measure the signals from several chemical species.

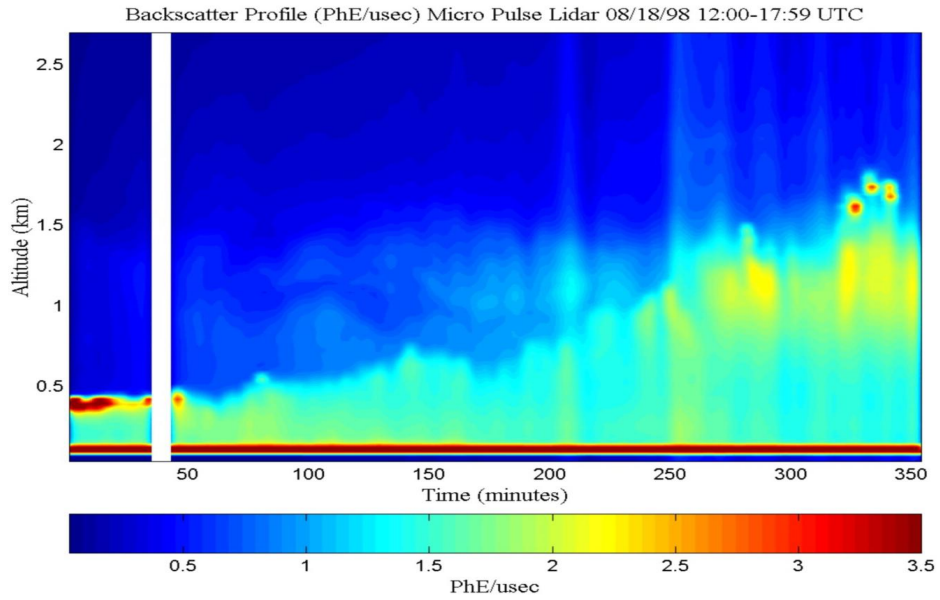

Figure 1. A time sequence of backscatter profiles during a 6-hr period from 8 AM to 2 PM shows the growth in thickness of the PBL during the morning hours and initial development of summer afternoon rain clouds [15].

An advantage of Raman lidar is that the signature can be measured using any laser wavelength in the visible or ultraviolet wavelengths. Figure 2(a) shows a diagram of the vibrational and rotational energy levels that are associated with Rayleigh and Raman scattering [13,14]. Rayleigh scattering (left side) occurs when a photon interacts with the vibrational ground state of a molecule, where most molecules reside at normal atmospheric temperatures, and the molecule scatters the photon at nearly the same energy. The scattered photon can be shifted slightly by the Doppler velocity of the molecule. Molecules that are Raman active, meaning that a phonon can induce change in polarizability and can scatter to a Stokes level, reducing the photon energy and leaving the molecule in an elevated vibrational level, resulting in a red-shifted photon. Since the vibrational energy states are unique to a molecule, the spectrum of Raman shifted Stokes transitions provide a fingerprint to identify the species present, and the intensity quantifies the concentration. If the molecule already exists in a higher vibrational level, it can undergo anti-Stokes scattering and takes with it the energy of the vibrational level, thus it is blue-shifted. The ranges Stokes and anti-Stokes wavelength bands for the Nd:YAG laser fundamental, and its harmonics, are shown in Fig. 3(a). The locations of wavelength shifts are shown for many common molecules in Fig. 3(b) [6]. The cross-sections for Raman scattering are small, Stokes scattering is a factor of thousands smaller than Rayleigh scattering, and anti-Stokes is even less likely because it requires the molecule to already be in a vibrational state (tenths of an eV), which is unlikely at normal atmospheric temperatures. Figure 2(a) also schematically shows a spectrum of the relative intensities of the scattering signals expected for a 2nd harmonic Nd:YAG laser at 532 nm. Note that rotational Raman bands (Stokes and anti-Stokes) are associated with each vibrational energy state. The ratio (660/607) of the vibrational Raman signals of water vapor and molecular nitrogen provide the signal to determine the water vapor concentration. The rotational Raman bands (Stokes and anti-Stokes) in Fig. 2(a) are shown in detail in Fig. 2(b) for a 532 nm laser scattering in air [14]. The rotational states are described by the Maxwell-Boltzman distribution for a gas in thermal equilibrium, and changes in the shape of that distribution describe the changes in temperature. The variation in the ratio of intensities in the rotational Raman energy levels for the signals at 528 nm and 530 nm provide a measurement of atmospheric temperature. By measuring the ratio of scattered signals at two wavelength pairs, 660/607 (H_2O/N_2) and 528/530 (two points on the temperature distribution of energy states), the water vapor and temperature profiles can be calculated. The measured ratios are used, together with the relative sensitivity of the two detectors (obtained by switching the input channels or using a standard source) and the laboratory values of cross-sections, to calculate the water vapor concentration profile, and a similar approach is used to obtain the temperature profile.

Figure 3(a) shows the Stokes and anti-Stokes bands of Raman scattering for an Nd:YAG laser and its harmonics. The figure indicates the range of the Raman scattered wavelengths. The frequency shifts expected for many molecular species are shown in Fig.3(b), and those shifts for N_2, O_2 and H_2O are indicated for an Nd:YAG laser [6].

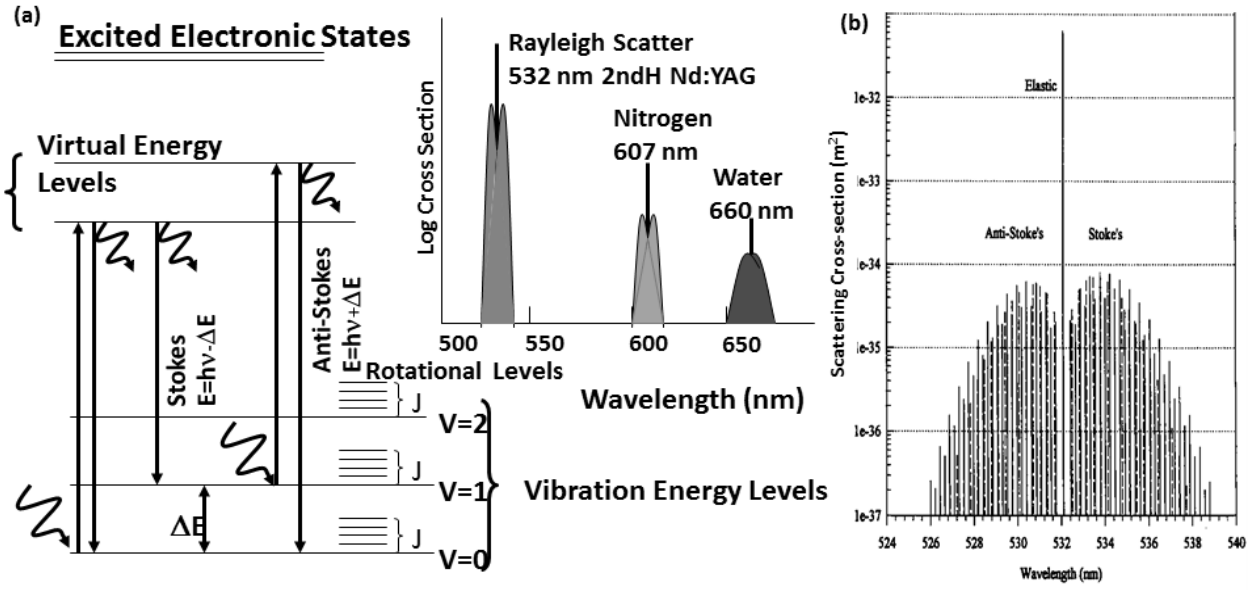

Figure 2. Raman lidar energy states: (a) schematic energy levels and spectra shows Rayleigh scattering and Raman scatter for Stokes and anti-Stokes components of an Nd:YAG laser 2nd harmonic at 532 nm [13-14], (b) the scattering cross-sections of the N_2 and O_2 rotational Raman lines around the 532 nm ($\Delta J = 0$) elastic scatter line [14].

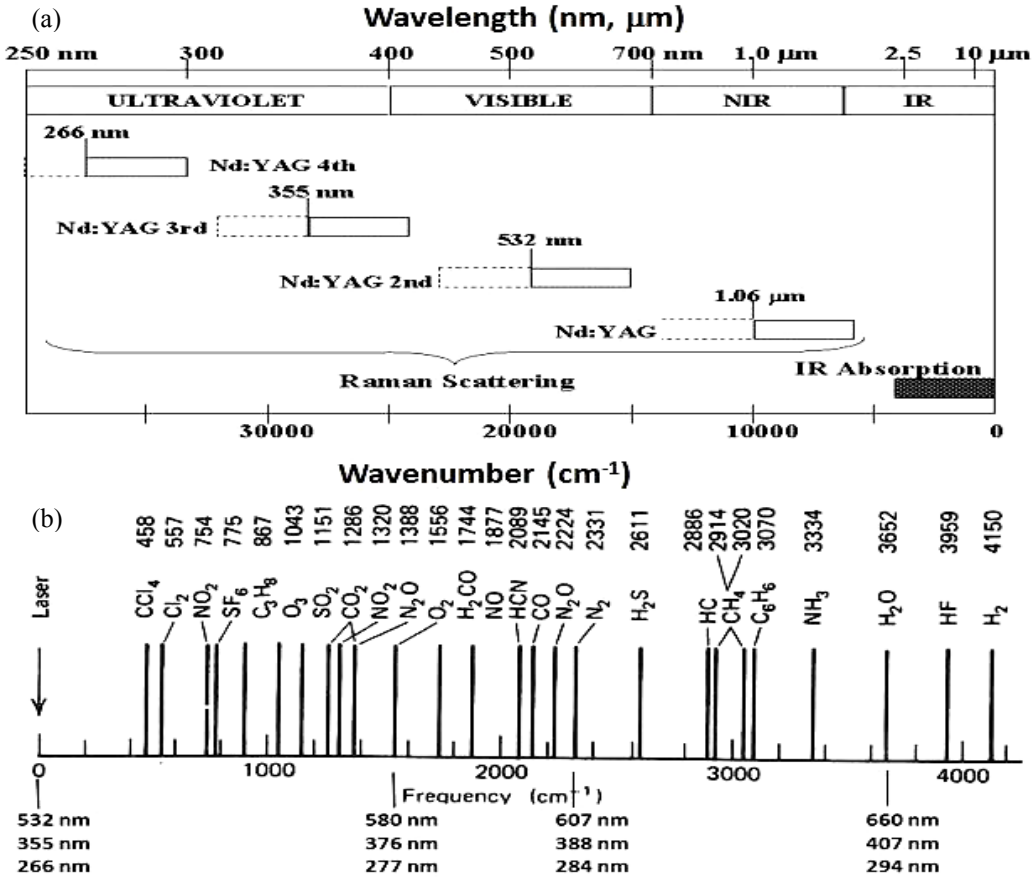

Figure 3. Raman signal intensity: (a) wavelength bands in which Stokes and anti-Stokes vibrational Raman scatter signals can be observed are shown for the 2nd, 3rd and 4th harmonics of the Nd:YAG laser, (b) frequency shifts for many common Raman active molecules are shown, and the expected wavelengths for the N_2, O_2, and H_2O molecules are indicated [6].

Another more subtle advantage of Raman measurements for atmospheric molecules is that the N_2 signal provides a good reference to determine the concentration for all of the Raman active species present. The scattering intensity for both Raleigh and Raman scattering depends on ν^4, and thus a laser at ultraviolet wavelengths has a signal detection advantage until atmospheric extinction becomes important. The species concentrations, temperature profiles, and aerosol optical properties can be measured. The aerosol optical extinction profiles are obtained from gradients in the measured molecular profiles, which include the vibrational Raman profiles of N_2, O_2, and the rotational lines near the band peaks, compared to the hydrostatic profile for atmospheric conditions. A major advantage of these Raman lidar techniques is that the quantitative values of optical efficiencies of the transmitters, receivers, and detectors are not needed.

Figure 4 shows an example of the water vapor profile measured with the LAMP Raman lidar at Pt. Mugu Naval Station CA in 1993 [14]. Measurements of specific humidity, or water vapor mixing ratios, are determined by taking the ratio of the signals from the vibrational Raman shift for water vapor and nitrogen. The profile in Fig. 4 shows a water vapor measurement with bars at ± 1 σ standard deviation. The water vapor profile that would be expected at 100% relative humidity is plotted from calculations using the measured temperature profile. To make lidar measurements during daylight conditions, the "solar blind" region of the spectrum between 260 and 300 nm is used. The “solar blind” region is darkened by the stratospheric ozone absorption of solar ultraviolet radiation. The visible channels (660/607) are available at night and the ultraviolet measurements (294/284) are used day and night [29]. The water vapor is a particularly important tracer of the tropospheric dynamics; it is the best indicator of the thickness of the planetary boundary layer, daytime convection processes, atmospheric waves and turbulence, and other dynamical features [25-33].

The temperature profile in Fig. 5 is measured from the ratio of signals at two wavelengths within the distribution of rotational states [14,26,30]. Band filters for rotational Raman signals near 527 nm and 530 nm in Fig. 5(b) are used to calculate the atmosphere temperature values that are shown at 75 m steps with ± 1 σ bars.

Raman lidar is particularly useful for describing the aerosol properties. Optical extinction includes contributions from both absorption by chemical species and scattering by molecules and particles. The Raman scatter profiles of the major molecular species can be used to calculate profiles of optical extinction. The gradients in the measured molecular profiles, at 607 nm (N_2), 530 nm ($N_2 + O_2$) and 284 nm (N_2) are used to calculate the extinction shown in Fig. 6 [14,35]. Comparison of optical extinction profiles at different wavelengths can be used to describe changes in the particle size distribution as a function of altitude. These measurements can then determine the air mass parameter, atmospheric optical density, and visibility. Optical extinction is determined from the gradient of the molecular profile compared with the expected molecular density gradient. Solving the lidar equation for the aerosol extinction uses the equations,

$$\alpha_R^{aer} = \frac{d}{dz}\left[\ln \frac{N_R(z)}{P_R(z)\cdot z^2}\right] - \alpha_0^{mol}(z) - \alpha_R^{mol}(z) - \alpha_0^{aer}(z)$$

$$\alpha_{532}^{aer} = \frac{d}{dz}\left[\frac{1}{2}\ln \frac{N(z)}{P_{530}(z)\cdot z^2}\right] - \alpha_{532}^{mol}(z) \quad .$$

O - outgoing - 532 or 266 nm

R - return - 530 (rot), 607 (N_2), 285 (N_2) or 276 (O_2) nm

The extinction profiles at 530, 607 and 284 nm measured in Philadelphia during NEOPS and in Hesperia during SCOS97 are shown in Fig. 6. The differences observed between the 530 nm and the 607 nm profiles, and the ultraviolet extinction are due to the size distribution of aerosols (the ozone absorption and molecular scattering are removed) [39-43]. The multiple scattering by the larger particles in the upper cloud layers removes the wavelength dependence.

The ozone profiles in the lower troposphere are measured using a DIAL analysis of the ratio of the vibrational Raman signals for nitrogen (284 nm) and oxygen (278 nm), which are on the steep side of the Hartley band of ozone [35-38]. The Raman shifts for N_2 and O_2 are used to calculate ozone profiles. Since the O_2/N_2 ratio in the lower atmosphere is constant to within about $1{:}10^5$, variations in the vertical profile of this ratio can be associated with absorption due to ozone. Figure 7 shows the lidar profiles of ozone measured by the LAPS lidar instrument and an aircraft point sensor while it circled the lidar beam during a set of measurements in the NEOPS program. The figure also shows the location of Raman shifted wavelengths on the sloping side of the Hartley band. The laboratory measured cross-sections are used in a DIAL lidar analysis to calculate the concentrations of ozone. The primary error source in the measurement depends only on the statistical error associated with the signal strength, it was typically 1 to 5 ppb below 1.5 km.

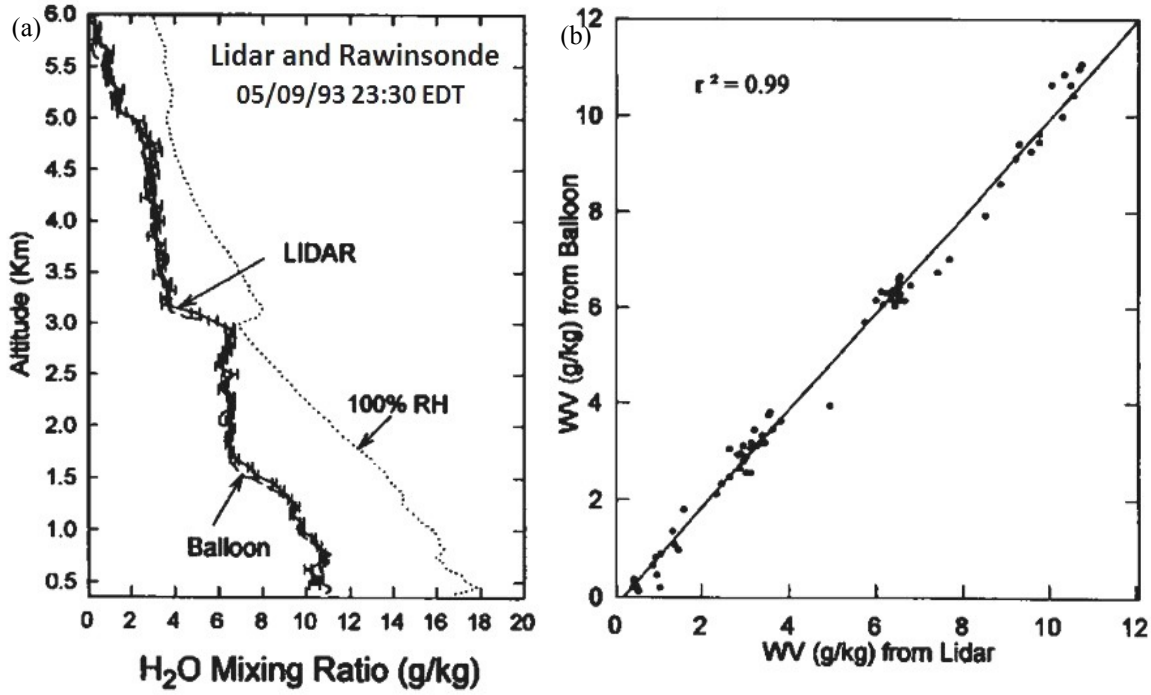

Figure 4. Raman lidar measurements of the water vapor mixing ratio compared with a rawinsonde balloon profile obtained simultaneously: (a) Vertical profiles of the lidar (75 m resolution) with $\pm$ 1 σ (standard deviation) bars on the profile, (b) plot shows the correlation coefficient between the lidar and rawinsonde balloon measurements [14,25].

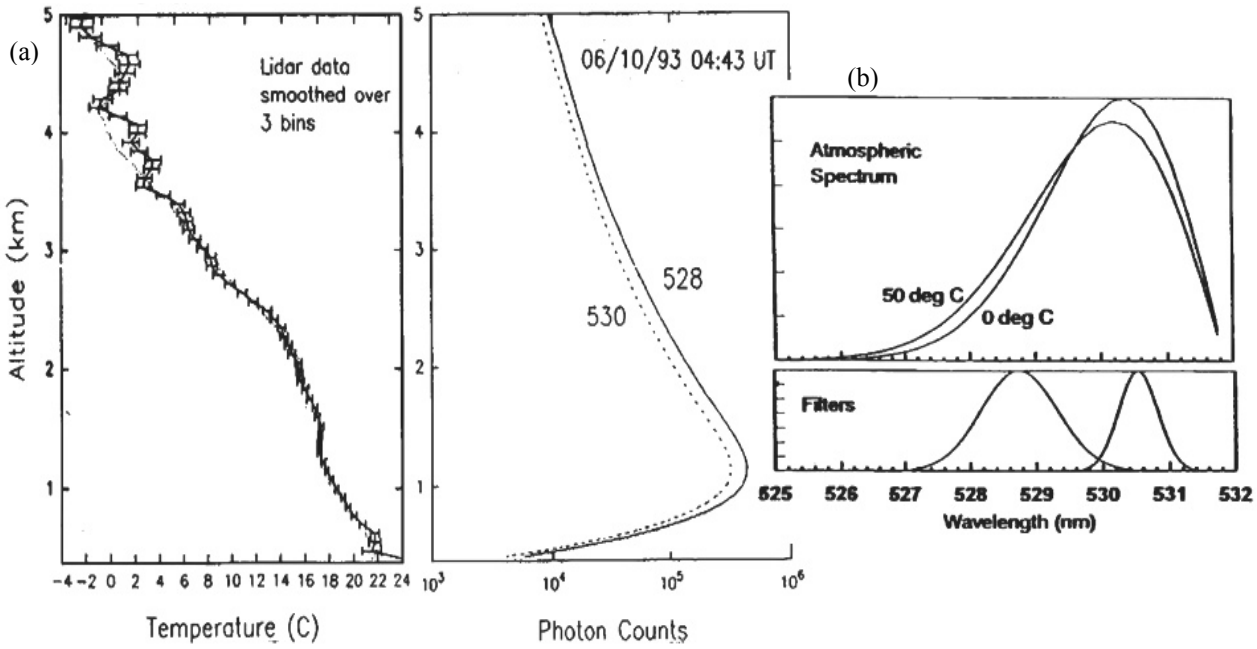

Figure 5. (a) Raman lidar temperature profile is compared with a simultaneous rawinsonde balloon, (b) temperature profile calculated from the ratio of 528 to 530 nm signal profiles for two narrow-band filter channel signals from the rotational lines in the anti-Stokes Raman rotational spectrum wing (see the rotational Raman spectrum in Fig. 2(b)) [14,26,30].

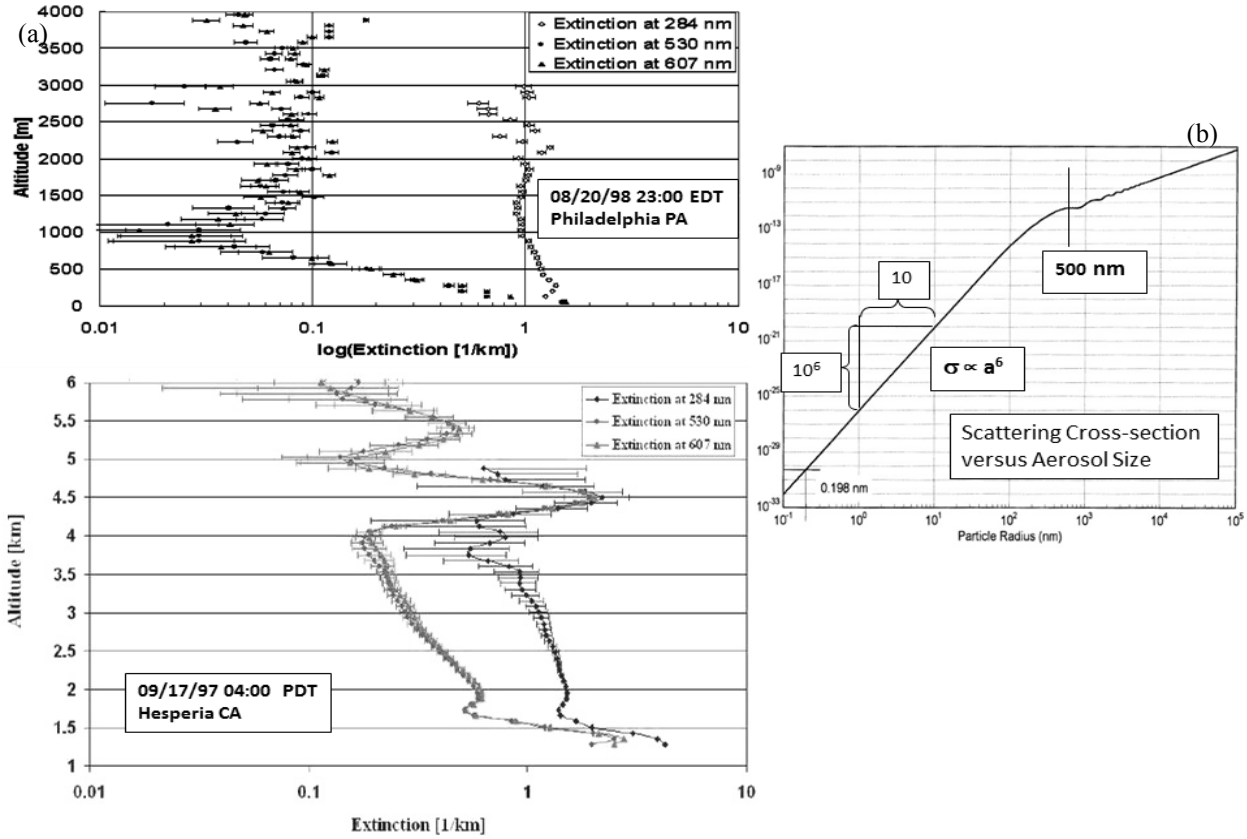

Figure 6. Optical extinction profiles at different wavelengths: (a) profiles exhibit a scattering cross-section dependence on particle size, aerosol density, and scattering wavelength, also the wavelength dependence shows whitening due to multiple scattering in cloud layers (~4.5 km), (b) scattering cross-section % a^6 for particle size <λ, and % a^2 when >λ [14,41–43].

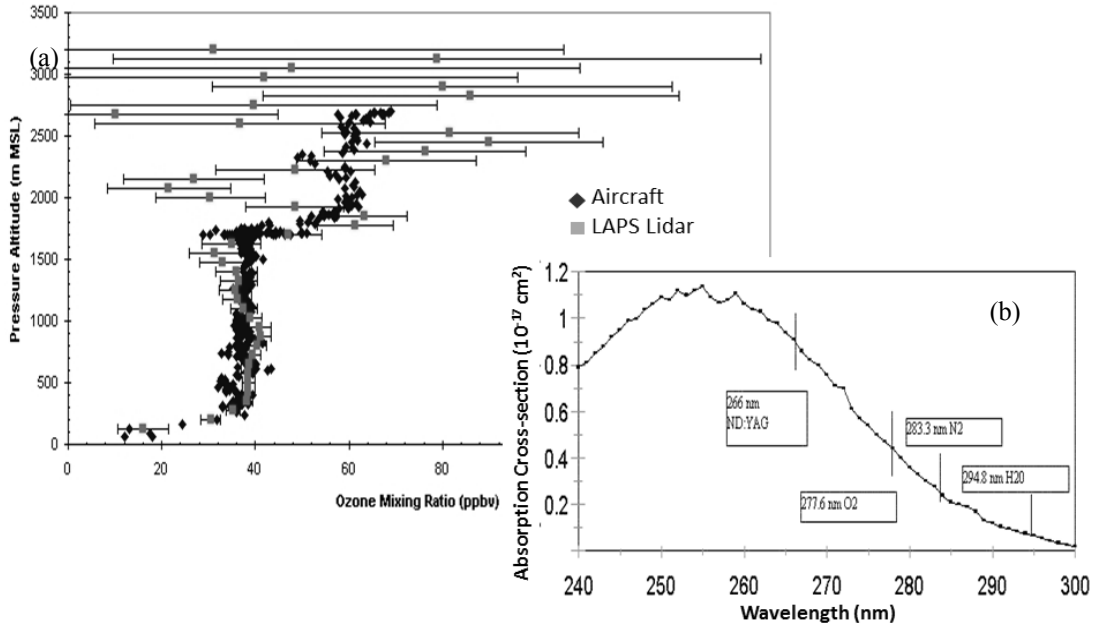

Figure 7. The ozone concentrations: (a) measured by Raman lidar with aircraft measurements provided by Bruce Doddridge, UMD, (b) the region of the DIAL analysis using the ratio of N_2 (283.3 nm) and O_2 (277.6 nm) shows absorption of Raman scatter signals on the steep side of the Hartley band of ozone [14,35-38].

3. STUDIES OF THE ATMOSPHERE

Lidar provides a special capability to make hundreds of profiles each day, and then profiles can be plotted in sequences to study the time variations of dynamical/chemical processes that control the atmosphere as it moves past the instrument location. Figure 8(a) shows three profile sequences of LAPS lidar aerosol optical extinction, ozone, and water vapor during a period of 24 hours when a significant air pollution event occurred at the Philadelphia NARSTO-NEOPS site [35,36]. Beginning at 8 AM EDT, the water vapor profiles shows the growth of the morning PBL (the outer scales of the convective eddies are observed), while moist air from the nighttime residual layer brings in a polluted air mass (back trajectory shows it came from Ohio Valley). When the PBL rises sufficiently, it rapidly transports the polluted air to the ground, where thermal decomposition of precursor chemicals (probably PAN) quickly produces smog and ozone by photochemistry. Notice that the water vapor data provides an effective tracer of dynamics during the period. Figure 8(b) shows profiles of water vapor when an instrumented aircraft circled the lidar beam and a rawinsonde balloon made measurements for comparison [14,37]. The aircraft data were obtained during the two periods indicated on the graph and compared below to the LAPS lidar profiles (with $\pm 1\ \sigma$ bars). The profile obtained with a rawinsonde balloon is compared with a lidar profile about 30 minutes earlier (see 3rd plot); however, a visual inspection shows that the two techniques agree well when compared in the same time interval as the balloon rises through a structured boundary layer. The value of continuous measurements using lidar is demonstrated in this data set. A meteorologist observing a continuous data set, such as that produced by the Raman lidar, has a much better grasp of the atmospheric conditions.

The Raman lidar 6-hour sequences of water vapor and temperature profiles measured in the Gulf of Mexico onboard the USNS Sumner in 1996 are plotted in Fig. 9 [14,15,56]. These profiles are used to calculate the relative humidity variations during the period (see top right-hand panel). The relative humidity shows higher values near the top of the boundary layer that can lead to cloud formation. An examination of the measured optical extinction by small particles during this period (see lower right panel) does show the formation of light clouds. Another interesting property that can be calculated from the same data is the RF refraction variations due to gradients in water vapor, and those can impact radar propagation [31,32].

One of the recent topics that we have explored is the possibility of using resonance Raman scattering to identify and measure the trace concentrations of selected species. We found that ***liquid*** aromatic compounds have the much unexpected property of a very strong resonance in Raman scattering when a tunable laser approaches and overlaps an electronic absorption feature in the ***vapor*** spectrum [50]. Figure 10(a) shows a portion of the vapor ultraviolet absorption spectrum of benzene, and Fig. 10(b) shows the intensity of the Raman scatter as a tunable OPO laser, which is illuminating benzene liquid from the bottom, is stepped across an absorption feature in the vapor spectrum [50]. The response is as if an instantaneous interaction of the photon with the molecule scatters without communication with neighboring molecules, whereas an optical spectrum of liquid benzene does not show any peak at that wavelength. This family of chemical species and others provide interesting subjects for future resonance Raman lidar investigations.

A 3-λ DIAL lidar was developed with ITT between 2002 and 2007 for aircraft measurements to detect natural gas pipeline leaks, and the ANGEL program then became a commercial service business [51]. Figure 11 shows the MWIR DIAL lidar instrumented aircraft, and two examples of measurements obtained during the testing program. The two panels on the right show the ground track of the aircraft, the top shows the laser shot pattern on the ground that was controlled by an on-board GPS pointing system aiming at the mapped coordinates of a buried pipeline. The lower panel shows the location of a potential leak, which was found in a coupling at that location. The lower left panel shows another case where the lidar scan pattern is centered on the map location of a buried pipeline, and two methane leaks are located, the scale indicates the concentration that the aircraft lidar detected.

Figure 12 shows one example of data from the new Supercontinuum Absorption Lidar (SAL), which has been used to measure the concentrations of gasses on long paths [52-54]. In this case, the water vapor concentration, measured in the 1420 to 1460 nm spectral band, is compared with the MODTRAN™5 spectrum, with the concentration adjusted to the measured value. The spectral features align well with the model calculation (the model must be adjusted to account for the index of refraction of air at this resolution). The wide spectrum of the supercontinuum laser can be used to perform a DIAL analysis of many on-line and off-line ratios, and repetitively, so accurate measurements are obtained. It can also measure trace species while avoiding any interfering contaminating species.

Figure 13 is given to inspire future investigations by showing a few cases with very interesting atmospheric features involving dynamical process which cannot be observed without the special ability of lidar to measure continuously.

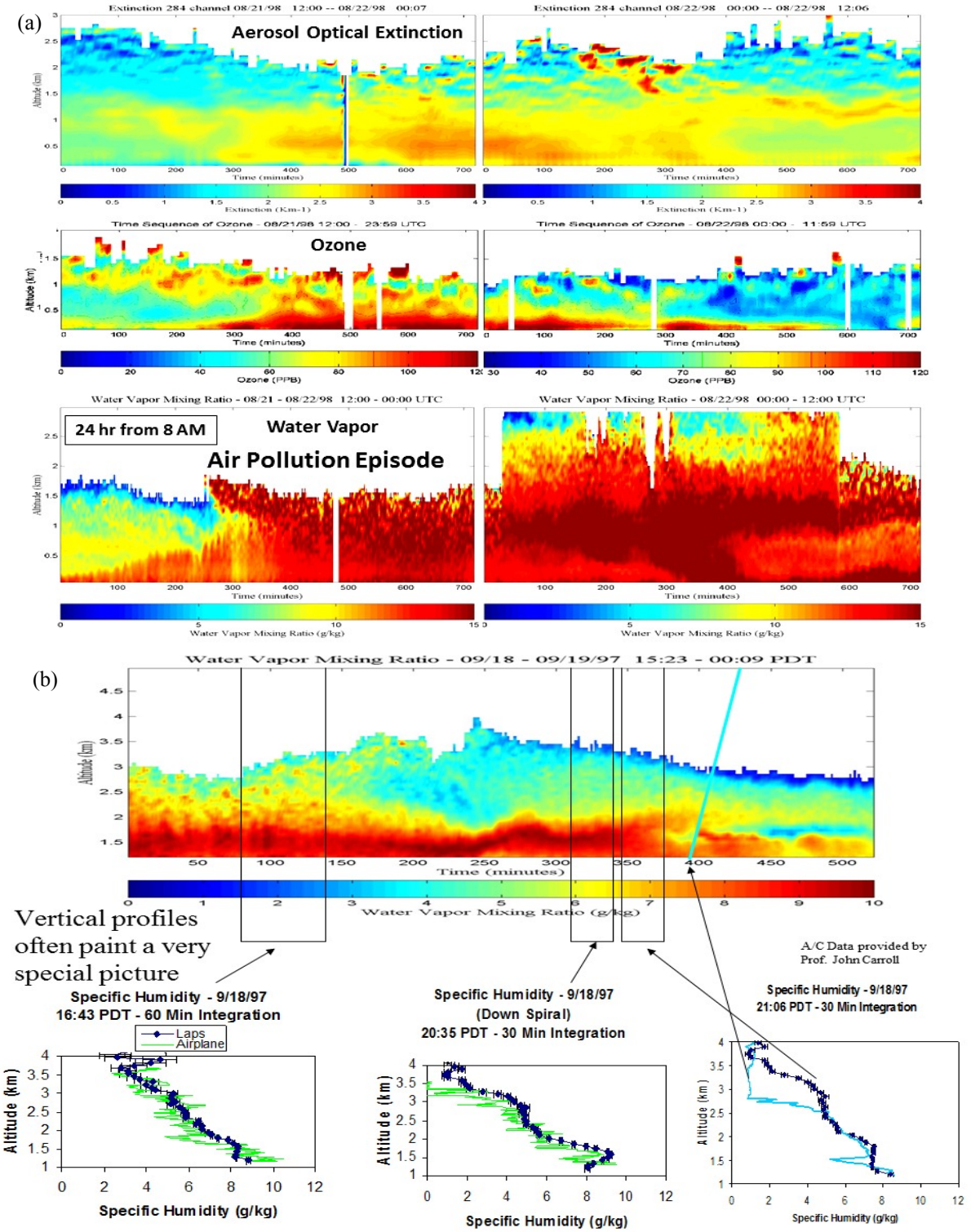

Figure 8. Time sequences of lidar profiles provide a unique lower atmosphere picture of the dynamics and chemistry: (a) 24-hour sequence from 8 AM EDT during an air pollution event [35], (b) water vapor profiles of Raman lidar, an aircraft instrument circling the laser beam, and a locally released rawinsonde balloon launch are compared to demonstrated water vapor as a useful tracer of dynamical processes (aircraft measurements provided by John Carroll, UC Davis) [14,35-37].

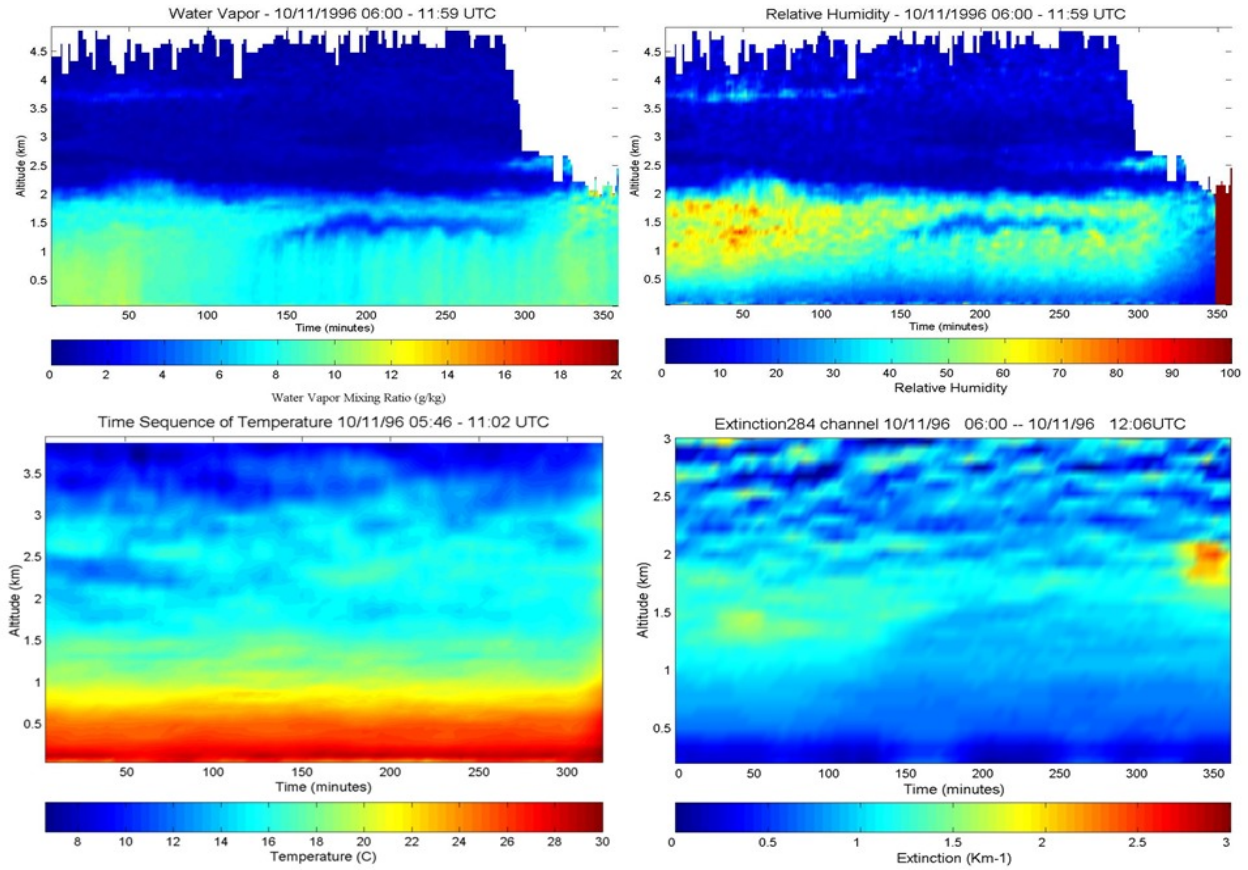

Figure 9. A six hour sequence of water vapor and temperature profiles are used to calculate relative humidity, which is compared with the UV optical extinction to observe the sub-visual development of clouds [14,15,56].

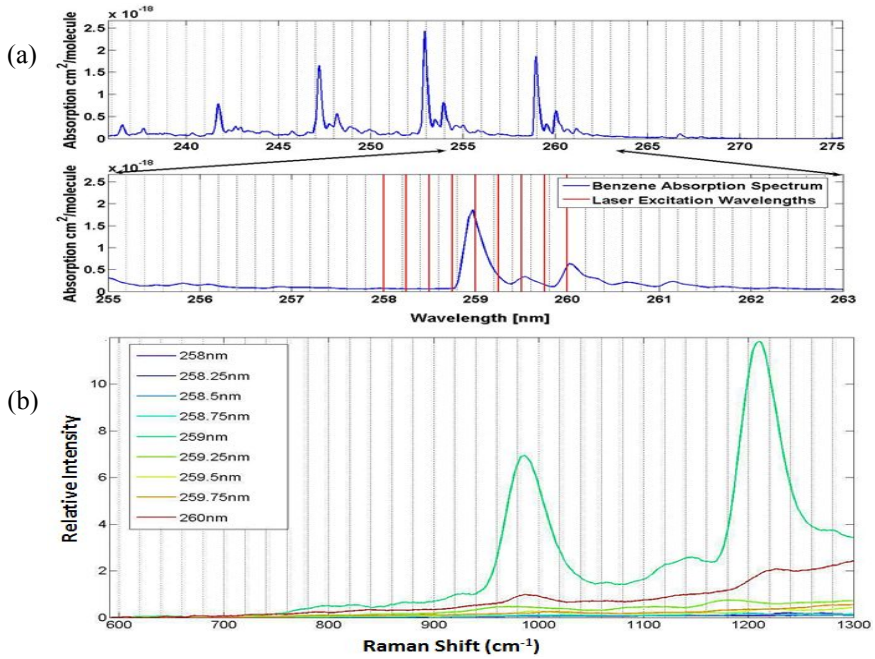

Figure 10. Resonance Raman scattering occurs: (a) at the vapor absorption (upper spectrum), (b) in liquid benzene with an amplification of 4000X, as a tunable UV laser steps over the vapor absorption wavelengths [50].

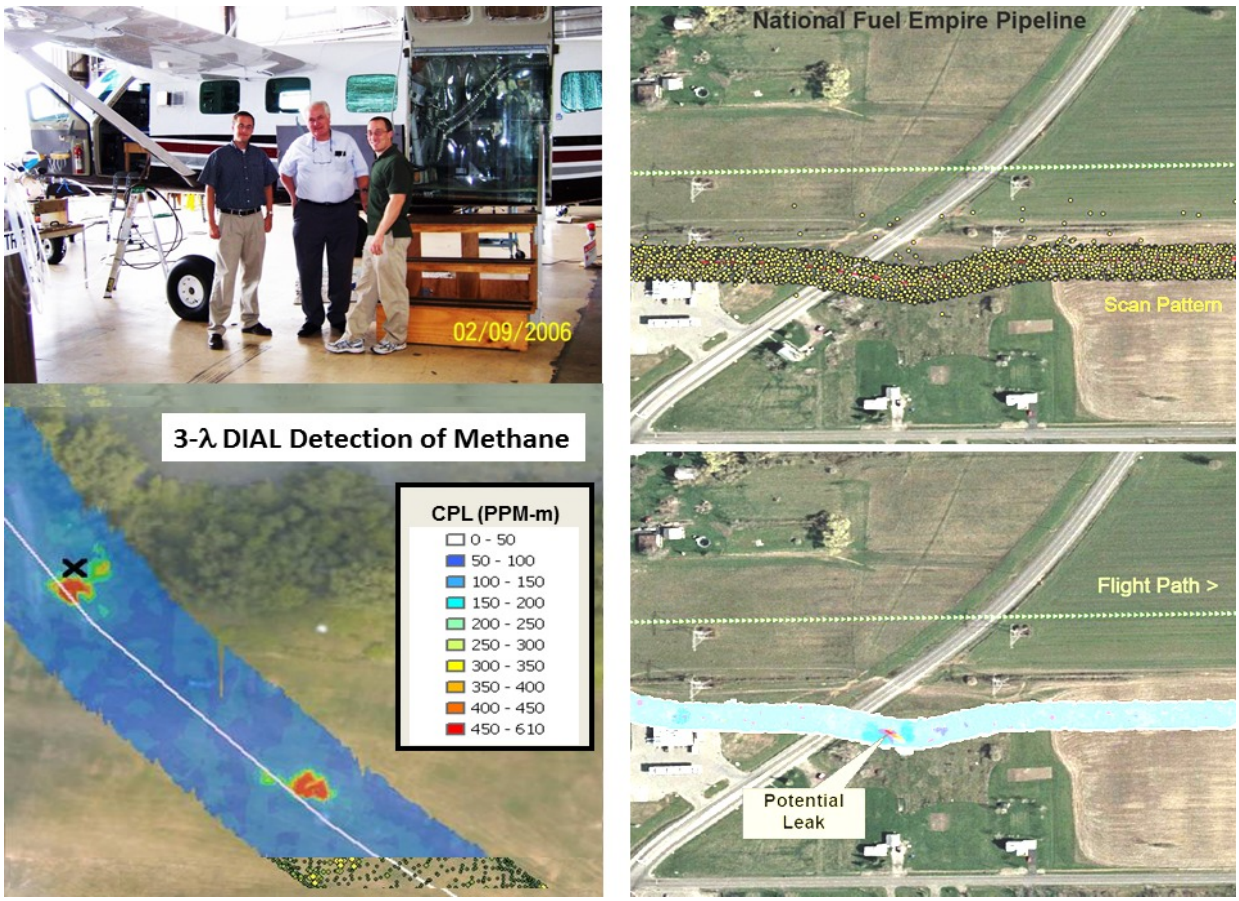

Figure 11. A DIAL lidar was developed to search for leaks in natural gas pipelines using a 3-λ OPA laser to measure methane in the 3 μm region. The lidar system (ANGEL) developed for ITT and now a commercial detection service [51].

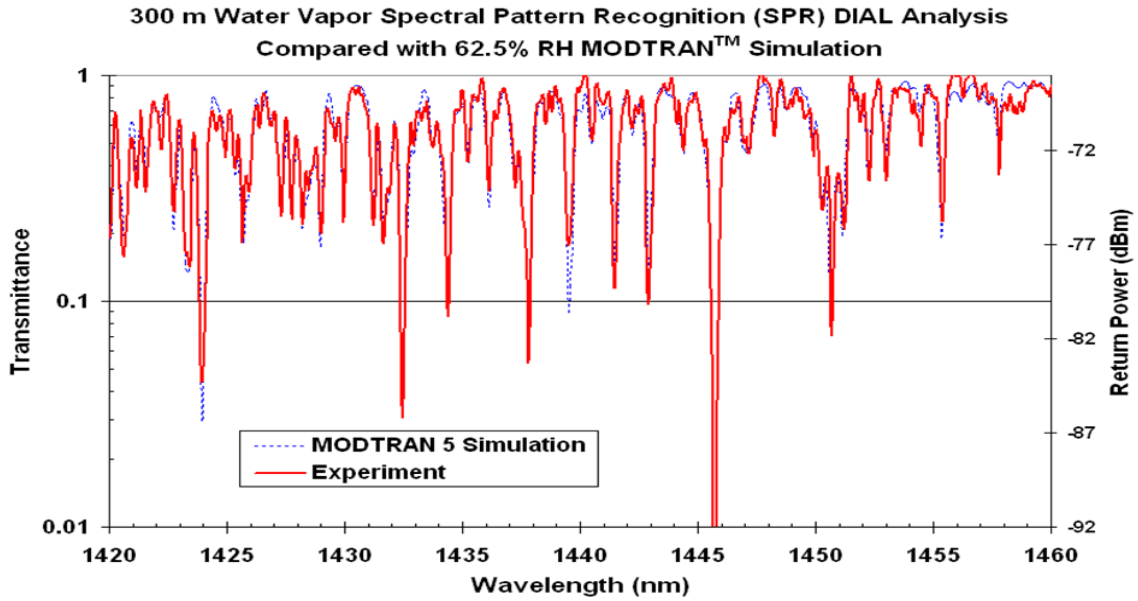

Figure 12. A supercontinuum laser has been used on long outdoor paths to measure several molecular species, here water vapor concentration was measured in a NIR absorption band. The advantage is that many on-line and off-line measurements are made simultaneously, and the presence of any interfering species is easily detected [52-54].

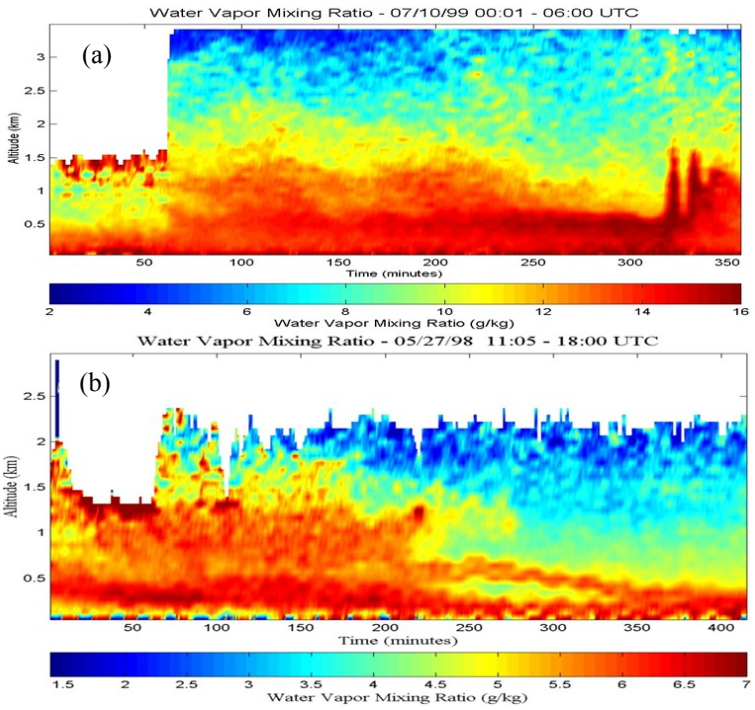

Figure 13. Interesting dynamical processes in the lower atmosphere: (a) Bore wave and gravity wave damping observed as a front passed the Raman lidar during a 6-hr data set between 8 PM and 2 AM LT on July 9-10 1999 at the EPA NARSTO-NEOPS field site in Philadelphia, (b) Buoyant oscillation forced by a pressure wave at the Brunt-Väisälä frequency observed at Point Barrow Alaska on 27 May 1998 4-10 AM LT during the arctic springtime (c) convective cloud development over the ocean 'sips' water vapor directly from the marine boundary layer, (d) observing the development of clouds with different wavelengths differentiate the smaller from the larger particles and indicates whether the cloud is in process of growth or dissipation [15,56].

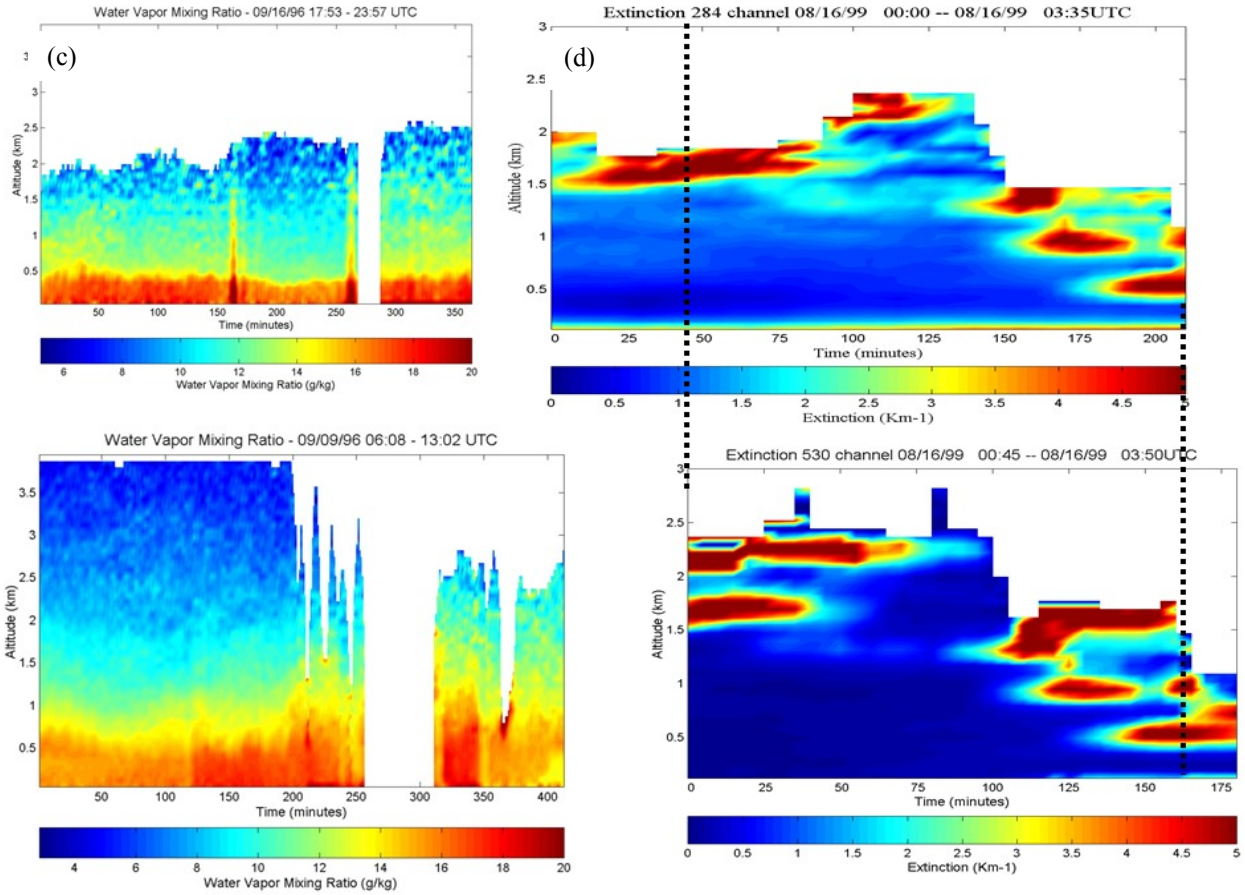

The cases shown in Fig.13 include several of the rarely observed features that should be studied to further help our understanding of these complex dynamical processes in the lower atmosphere, and it includes an example from a study of cloud evolution [55,56,58]. An interesting observation was already pointed out in Fig. 8(a), the water vapor data shows the outer scale of the ***convective cells*** growing to form the daytime boundary layer. Figure 13(a) shows an ***internal bore wave*** occurrence during a 6-hour sequence of water vapor profiles on the night that followed a major air pollution event at the Philadelphia NEOPS field site. The feature appears as a damped pressure wave. It coincided with the passage of a low pressure front through the area. Another event similar was studied 25 years earlier using a Raman lidar [57]. Figure 13(b) shows a ***buoyant oscillation*** forced at the Brunt-Väisälä frequency that we observed at Point Barrow Alaska on 27 May 1998 4-10 AM local time during the arctic springtime. The fact that the oscillation occurred for a long period suggests that the source may have provided energy into the atmosphere for a more extended period than the oscillation shown in Fig. 13(a) that damped more quickly. Figure 13(c) shows two data sets when moisture was effectively transferred into the base of forming clouds from the marine boundary layer. The measurements were made as the LAPS lidar traveled through the Gulf of Mexico onboard the USNS Sumner in 1996. The convection appears to be '***sipping***' water from the marine boundary layer. Figure 13(d) shows the profiles of the optical extinction at two wavelengths as the aerosols contribute to cloud formation. At the same time, the Raman lidar measured profiles of water vapor and temperature. By combining these types of data with measurements of the lidar measurements of phase changes in the water, we hope to extend the work of Verghese [58]. These studies are needed to fully understand the microphysical processes in clouds. This figure also shows the multiple scatter, or 'whitening,' of the two-color extinction in the clouds. The signatures show the changes in particle size and density in the vicinity of the clouds.

While examining the many different atmospheric properties that can be simultaneously measured using Raman lidar techniques, it is easy to forecast that these types of measurements will be at the forefront of the research to understand atmospheric processes during the years ahead. As we come to face the climate changes, which are only just beginning, the Raman lidar provides a useful tool to examine and understand the atmospheric processes needed to help us make the right policy decisions to minimize risk and damage to our environment.

ACKNOWLEDGMENTS

The following organizations and individuals are acknowledged for support of the lidar development at Penn State University, shipboard tests, and field campaigns: US Navy through SPAWAR Systems Division, PMW-185, NAVOCEANO, NAWC Point Mugu, and ONR; also to DOE, EPA (STAR Grant R826373), California Air Resource Board, NASA and NSF. The NARSTO-NEOPS air quality investigations were supported by USEPA STAR Grants with assistance from Pennsylvania DEP and MARAMA. Special appreciation goes to D. Sipler, G. Davidson, C. S. Gardner, U. vonZahn, D. B. Lysak, F. Balsiger, T. M. Petach, J. Jenness, T. J. Kane, Z. Liu, D. M. Blood, B. Chen, T. D. Stevens, P. A. T. Haris, M. D. O'Brien, D. Machuga, T. Manning, S. Sprague, G. OMarr, A. Achey, A. Nanduri, J. Park, C. Bas, J. Begnoche, R. Harris, P. J. Collier, T. Manning, G. Evanisko, S. Boone, G. Chadha, S. Unni, S. Kizhakkemadam, J. Collier, L. Liu, G. OMarr, S. Mathur, C. Slick, S. Sprague, A. Venkattarao, B. Mathason, S. Maruvada, D. Machuga, S. Rajan, M. Zugger, G. Evanisko, J. Yurack, S. T. Esposito, K. Mulik, A. Achey, E. Novitsky, Y.-C. Rau, G. Li, S. Verghese, A. H. Willitsford, D. M. Brown, A. Wyant, D. M. Edwards, M. Snyder for their outstanding technical contributions to the developments of the Raman lidar technology. The contributions of colleagues Rich Clark, S.T. Rao, George Allen, Bill Ryan, Bruce Doddridge, D. Killinger, Steve McDow, Delbert Eatough, Susan Weirman, Bart Croes, C. Richey, M. Thomas, S. V. Stearns, J. Lentz, Dennis Fitz and are greatfully acknowledged.

REFERENCES

[1] Leonard, D. A., "Observation of Raman scattering from the atmosphere using a pulsed nitrogen ultraviolet laser," Nature 216, 142-143 (1967).

[2] Cooney, J. A., "Measurements on the Raman component of laser atmospheric backscatter," Appl. Phys. Lett., 12, 40-42 (1968).

[3] Melfi, S. H., Lawrence Jr., J. D., and McCormick, M. P., "Observation of Raman scattering by water vapor in the atmosphere," Appl. Phys. Lett. 15, 295-297 (1969).

[4] Cooney, J. A., "Remote measurement of atmospheric water vapor profiles using the Raman component of laser backscatter," J. Appl. Meteor. 9, 182-184 (1970).

[5] Cooney, J. A., "Comparisons of water vapor profiles obtained by rawinsonde and laser backscatter," J. Appl. Meteor., *2,* 301 (1971).

[6] Inaba, H., and Kobayasi, T., "Laser-Raman Radar," Optoelectronics, 4, 101-123 (1972).
[7] Strauch, R. G., Den, V. E., and Cupp, R. E., "Atmospheric water vapor measurement by Raman lidar," Remote Sens. Envir. 2, 101-108 (1972).
[8] Grant, W. B., "Differential absorption and Raman lidar for water vapor profile measurements: a review," Optical Engineering 30, 40-48 (1991).
[9] Arshinov, Yu. F., Bobrovnikov, S. M., Zuev, V. E., and Mitev, V. M., "Atmospheric temperature measurements using a pure rotational Raman lidar," Appl. Optics 22, 2984-2990 (1983).
[10] Vaughan, G., Wareing, D. P., Thomas, L., and Mitev, V., "Humidity measurements in the free troposphere using Raman backscatter," Q. J. R. Meteorol. Soc., 114, 1471-1484 (1988).
[11] Renaut, D., and Capitini, R., "Boundary-layer water vapor probing with a solar-blind Raman lidar: validations, meteorological observations and prospects," J. Atmos. Oceanic Tech. 5, 585-601 (1988).
[12] Melfi, S. H., D. Whiteman and R. Ferrare, "Observations of atmospheric fronts using Raman lidar moisture measurements," J. Appl. Meteo., 28, 789-806 (1989).
[13] Philbrick, C. R., "Overview of Raman lidar techniques for air pollution measurements," Proc. SPIE 4484, 136-150 (2002).
[14] Philbrick, C. R., "Raman Lidar Characterization of the Meteorological, Electromagnetic, and Electro-optical Properties of the Atmosphere," Proc. SPIE 5887, 85-99 (2005).
[15] Philbrick, C. R., Hallen, H., Snyder, M., and Brown, A., "Remote sensing of atmospheric aerosol properties," Proc. 91st AMS, Conf. Aer.l Prop., (2011). https://ams.confex.com/ams/91Annual/webprogram/13ATCHEM.html
[16] Philbrick. C. R., "Lidar profiles of atmospheric structure properties," Proc. SPIE 1492, 76-84 (1991).
[17] Philbrick, C. R., Lysak, D. B., Stevens, T. D., Haris, P. A. T., and Rau, Y.-C., "Atmospheric Measurements Using the LAMP Lidar during the LADIMAS Campaign," 16th ILRC, NASA Pub. 3158, 651-654 (1992).
[18] Philbrick, C. R., and Chen, B., "Transmission of gravity waves and planetary waves in the middle atmosphere based on lidar and rocket measurements," Adv. Space Res. 12(10), 303-306 (1992).
[19] Stevens, T. D., Maruvada, S., Kane, T. J., and Philbrick, C. R., "Lidar observations of Mt. Pinatubo aerosols: Effects on the global radiation budget," Proc. OSA 6th Opt. Rem. Sensing Atmos. 5, 313-316 (1993).
[20] Philbrick C. R., Lysak, D. B., Stevens, T. D., Haris, P.A.T., and Rau, Y.-C., "Lidar measurements of middle and lower atmosphere properties during the LADIMAS campaign," Proc. 11th ESA Sy., ESA-SP-355, 223-228 (1994).
[21] Stevens, T. D., Haris, P.A.T., Rau, Y.-C., and Philbrick, C. R., "Latitudinal lidar mapping of stratospheric particle layers," Adv. Space Res. 14(9), 193-198 (1994).
[22] Haris, P. A. T., Stevens, T. D., Maruvada, S., and Philbrick, C. R., "Latitude Variation of Middle Atmosphere Temperatures," Adv. Space Res., 14, (9)83-(9)87 (1994).
[23] Whiteman, D. N., Melfi, S. H., and Ferrare, R. A., "Raman lidar system for the measurement of water vapor and aerosols in the Earth's atmosphere," Appl. Optics 31, 3068-3082 (1992).
[24] Hauchecorne, A., Chanin, M. L., Keckhut, P., and Nedeljkovic, D., "Lidar monitoring of the temperature in the middle and lower atmosphere," Appl. Phys. B55, 29-34 (1992).
[25] Rajan, S., Kane, T. J., and Philbrick, C. R., "Multiple-wavelength Raman lidar measurements of atmospheric water vapor," Geophys. Res. Let. 21, 2499-2502 (1994).
[26] Haris, P. A. T., and Philbrick, C. R., "Rotational Raman lidar for temperature measurements in the troposphere," Proc. IEEE Topical Symp. COMEAS 10.1109, 141-144 (1995).
[27] Nedeljkovic, D., Hauchecorne, A., and Chanin, M. L., "Rotational Raman lidar to measure the temperature from the ground to 30 km," IEEE Trans. Geos. Remote Sens. 31, 90-101 (1993).
[28] Philbrick, C. R., "Raman lidar measurements of atmospheric properties," SPIE 2222, 922-931 (1994);
[29] Balsiger, F., and C. R. Philbrick, "Comparison of lidar water vapor measurements using Raman scatter at 266 nm and 532 nm," SPIE Proc. 2833, 231-240 (1996).
[30] Balsiger, F., P. A. T. Haris and C. R. Philbrick, "Lower-tropospheric temperature measurements using a rotational Raman lidar," SPIE Proc. 2832, 53-60 (1996).
[31] Philbrick, C. R., and Blood, D. W., "Lidar measurements of refractive propagation effects," [Propagation Assessment in Coastal Environments], NATO-AGARD CP 567(3), 1-13 (1994).
[32] Willitsford, A. H., and Philbrick , C. R., "Lidar Description of the Evaporative Duct in Ocean Environments," Proc. SPIE 5885, 140-147 (2005).
[33] Philbrick, C. R., "Raman Lidar Capability to Measure Tropospheric Properties," Proc. 19th ILRC, NASA/CP-1998-207671/PT1, 289-292 (1998).

[34] Vaughan, G., D. P. Wareing, D. P., Pepier, S. J., Thomas, L., and Mitev, V., "Atmospheric temperature measurements made by rotational Raman scattering," Appl. Opt. 32(15), 2758-2764 (2000).
[35] Philbrick, C. R., and Mulik, K., "Application of Raman lidar to air quality measurements," Proc. SPIE 4035, 22-33 (2000).
[36] Mulik, K.R., and Philbrick, C.R., "Raman lidar measurements of ozone during pollution events," Proc. 20th ILRC, 443-446 (2001).
[37] Philbrick, C. R., "Raman Lidar Descriptions of Lower Atmosphere Processes," Proc. 21st ILRC, 535-545, 2002.
[38] Esposito, S. T., and Philbrick, C. R., "Raman/DIAL Technique for Ozone Measurements," Proc. 19th ILRC, NASA/CP-1998-207671/PT1, 407-410 (1998).
[39] Philbrick, C. R., Hans Hallen, "Measurements of contributors to atmospheric climate change," Proc. 19th Symposium on European Rocket and Related Research, ESA SP-671 (2009).
[40] O'Brien, M. D., Evanisko, G. R., and Philbrick, C. R., "Initial results from a volume scanning three wavelength polarization lidar," Proc. IEEE Topical Symp. COMEAS 10.1109, 135-137 (1995).
[41] O'Brien, M. D., Stevens, T. D., and Philbrick, C. R., "Optical extinction from Raman lidar measurements," Proc. SPIE 2832, 45-52 (1996).
[42] Li, G. and Philbrick, C. R., "Lidar Measurements of Airborne Particulate Matter," SPIE 4893-15, 2002.
[43] Li, G., and Philbrick, C. R., "Study of Airborne Particulate Matter Using Multi-wavelength Raman Lidar," Proc. 22nd ILRC, ESA SP-561, 377-380 (2004).
[44] Stevens, T. D., and Philbrick, C. R., "Atmospheric extinction from Raman lidar and a bi-static remote receiver," Proc. IEEE Topical Symp. COMEAS 10.1109, 170-173 (1995).
[45] Novitsky, E. J., and Philbrick, C.R., "A Multistatic Receiver for Monitoring Lower Troposphere Aerosols and Particulate Matter," Proc. 22nd ILRC, ESA SP-561, 219-222 (2004).
[46] Novitsky, E. J., and Philbrick, C.R., "Multistatic Lidar Profiling of Urban Atmospheric Aerosols," J. Geophy. Res. Atmos. 110, DO7S11 (2005).
[47] Wyant, A. M., Brown, D. M., Edwards, P. S., and Philbrick, C. R., "Multi-wavelength, multi-angular lidar for aerosol characterization," Proc. SPIE 7323, (8 pages) (2009) doi: 10.1117/12.818686
[48] Wyant, A. M., Snyder, M. and Philbrick, C. R., "Multi-wavelength, multi-angular characterization of aerosols," Proc. SPIE 7684-17 (2010).
[49] Philbrick, C.R., Wyant, A.M., Verghese, S., Edwards, P.S. and Wright, T., "Characteristics of atmospheric aerosols based on optical remote sensing," Proc. 90th AMS, 12th Conf. Atmospheric Chemistry (2010). http://ams.confex.com/ams/90annual/techprogram/paper_163441.htm
[50] Willitsford, A. H., Chadwick, C. T., Hallen, H. D., Philbrick, C. R., "Resonance Raman measurements utilizing a deep UV source," SPIE, Proc. 6950, 69500A (2008) DOI: 10.1117/12.778253
[51] Murdock, D. G., Stearns, S. V., Lines, R. T., Lenz, D., Brown, D. M., and Philbrick, C. R., "Applications of Real-World Gas Detection: Airborne Natural Gas Emission Lidar (ANGEL) System," J. Applied Remote Sensing, 2, 023518 (2008). DOI:10.1117/1.2937078
[52] Brown, D. M., Liu, Z., and Philbrick, C. R., "Supercontinuum lidar applications for measurements of atmospheric constituents" Proc. SPIE 6950, 69500B-1 (2008). DOI: 10.1117/12.778255
[53] Brown, D. M., Shi, K., Liu, Z., and Philbrick, C. R., "Long-path supercontinuum absorption spectroscopy for measurement of atmospheric constituents," Opt. Exp. 16(12), 8457-8471 (2008)
[54] Edwards, P. S., Wyant, A. M., Brown, D. M., Liu, Z., Philbrick, C. R., "Supercontinuum laser sensing of atmospheric constituents," Proc. SPIE 7323, 73230S (8 pages) (2009), doi: 10.1117/12.818697
[55] Verghese, S. J., Willitsford, A. H., and Philbrick, C. R., "Raman Lidar Measurements of Aerosol Distribution and Cloud Properties," Proc. SPIE 5887, 100-107 (2005).
[56] Philbrick, C. R., Hallen, H., Brown, A., Wright, T., and Snyder, M., "Optical Remote Sensing Techniques Characterize the Properties of Atmospheric Aerosols," Proc. SPIE 7684-18 (2010).
[57] Koch, S. E., Dorian, P. B., Ferrare, R., Melfi, S. H., Skillman, W. C., and Whiteman, D., "Atructure of an internal bore and dissipating gravity current as revealed by Raman lidar," Mo. Weather Rev. 119(4), 857-887 (1981).
[58] Verghese, S. J., "Investigation of aerosol and cloud properties using multi-wavelength Raman lidar measurements," PhD Dissertation, Dept. Elect. Engr., Penn State University, University Park PA 16801 (2008).